

Design and Analysis of The CMOS Spatial Light Modulators with Flat Beam Profiles

Chen-Peng Hsu, Chih-Tsung Shih, Shih-Yi Wen, Yu-Han Chien, Chao-Chang Hu and Hsiao-Wen Lee

Industrial Technology Research Institute, Opto-Electronics & Systems Laboratories
195 Sec. 4, Chung Hsing Rd. Chutung, Hsinchu, Taiwan, CPHsu@itri.org.tw

ABSTRACT

Two new types of electrostatic grating light modulators (GLMs) are proposed, designed, and analyzed here. To improve optical wavefront distortion, the proposed GLMs are designed to provide flat reflective surfaces. The gratings consist of parallel rows of rigid microbeam structures with spring-like legs on beam-ends. For 200 μm long beams, the proposed designs achieve radius of curvature up to 200-900mm that can provide flat reflective surfaces. In optical simulation, the effect of bottom electrode reflection is considered to obtain the real diffractive phenomenon. Simulation results show the proposed GLMs improve wavefront distortion significantly. The optimal gap-size between ribbons is found also.

Keywords: MOEMS diffraction grating, spatial light modulator, wavefront distortion, CMOS MEMS

1 INTRODUCTION

The grating-type light modulator is a microelectromechanical phase grating made from parallel rows of reflective ribbons. It is employed for light switching and light intensity modulation by diffraction and is promising for MOEMS applications such as display and printing [1,2]. All the ribbons are electrically conductive and optically reflective. The ribbons are suspended over an air gap and are deflected downward by electrostatic force. When all ribbons are in the same plane, the ribbons reflect incident light normal to the surfaces like a mirror. When the alternate ribbons are pulled down, square wells are formed and then the incident light is diffracted at a specific angle.

The existence of inter-ribbon gap, the spacing between ribbons, can't be avoided for micromechanical devices; therefore the dimension of the spacing should be taken into consideration of design. In general, increasing inter-ribbon gap will reduce fill factor and results in lower diffraction efficiency [2] and contrast.

In addition, the deflected ribbons are in fact in curved shapes, hence the ideal square well diffraction pattern is no longer achieved and the intensity contours will be changed due to wavefront distortion [3]. To obtain flat reflective surfaces, ribbons with partial surface electrodes are employed by decreasing the percentage of the partial electrode coverage [4]. However, the electrostatic force is reduced significantly resulting in higher actuation voltage. In this work, two types of ribbon designs are proposed to achieve flat beam profiles. The proposed designs consist of

multi-layered structures and require fabrication process with submicron resolution. Among microfabrication technologies, the CMOS MEMS process fulfills the needs. The design and simulation of the proposed devices are based on the design rules and fabrication limitations of the CMOS process used. The geometrical parameters and electro-mechanical behaviors are simulated and discussed. Optical simulations are conducted to obtain real diffraction phenomenon and the results show the proposed designs improve the wavefront distortion significantly.

2 DEVICE STRUCTURE DESIGN

To achieve flat beam profiles, two new types of electrostatic microactuators are proposed to compose the grating light modulators, GLM2 and GLM3, as shown in figure 1. The clamped-clamped beam actuator used by conventional GLM (GLM1) is also shown as a comparison. Both of the microactuators consist of central microbeam portions with spring-like legs on the two beam-ends. The central microbeams are designed to have larger flexural rigidity by increasing the central beam thickness or moment of inertia. In operation, the spring-like legs will absorb most strain energy when the whole structure is attracted by electrostatic force and bend toward fixed electrode. Hence the central beam is almost un-deformed and can provide flat reflecting surface. For GLM2, the central beam portion is composed of stacked layers to increase the rigidity and form a parallel capacitor with the bottom planar electrode. For GLM3, the central beam is T-shaped in cross-section that forms a vertical comb drive with the bottom U-shaped electrode. In general, the number of spring-like legs can be adjusted in pairs to modify the electro-mechanical response of the microactuators.

The proposed multilayered devices require fabrication process with multi structural layer, well-controlled film thickness and sub-micron linewidth resolution. Therefore, the CMOS fabrication process that provides multilevel interconnection (MLI) technology fulfills the needs. Here, the TSMC 0.35 μm mixed-signal 2P4M process is used to fabricate the devices with minimal gap size of the grating down to 0.6 μm . The process provides four metal layers to fabricate the CMOS MEMS structures. The post CMOS process is conducted with wet etchant and drying by supercritical CO₂ dryer. The intermediate dielectrics layers (IMD) are used as sacrificial layers and removed selectively by commercial etchant Pad Etch I (Ashland). Figure 2 shows SEM photomicrographs of the fabricated CMOS grating light modulators. Where the beam widths of the

GLM1 and GLM2 are $3\mu\text{m}$ and that of the GLM3 is $4\mu\text{m}$. The gaps between beams, called as inter-ribbon gap in this work, are $1\mu\text{m}$.

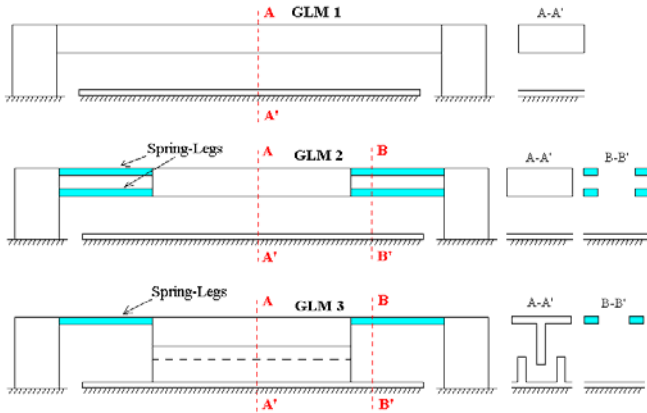


Figure 1: Schematic drawings of the proposed electrostatic microactuators for GLM2 and GLM3. Where GLM 1 is the conventional clamped-clamped beam actuator.

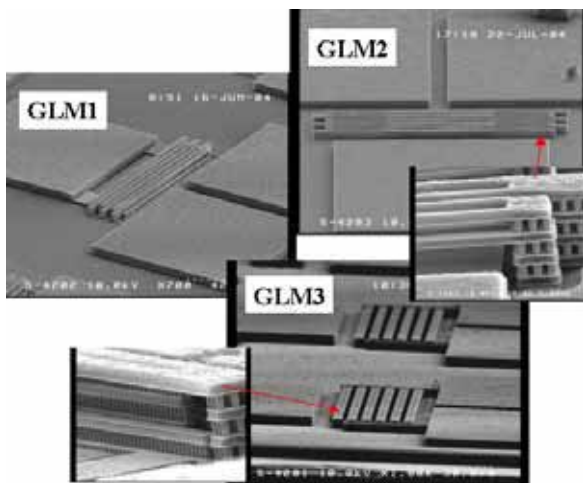


Figure 2: SEM photomicrographs of the fabricated CMOS grating light modulators, GLM1, GLM2, and GLM3.

3 ELECTRO-MECHANICAL SIMULATIONS

The electrostatic-structural analyses are performed by using ANSYS 8.0. The method of sequentially coupled physics analysis with physics environment approach is used to solve the fully coupled model. The mechanical structural is meshed with SOLID95 brick elements and the air is meshed with SOLID122 tetrahedral elements to solve the electric field distribution.

The geometrical dimensions of spring-like leg are important in mechanical design. The length and width of the leg are considered in analysis. In fact, the thickness is crucial to the mechanical behavior of the device. However, the thickness of the CMOS metal-interconnection process is

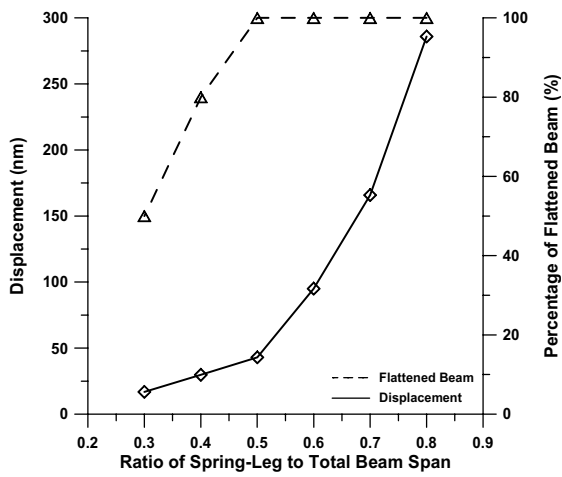
restricted and therefore all values of thickness are fixed in simulation. The movable parts of the devices are fabricated on metal 4, metal 3 and metal 2 layers with thickness of $0.925\mu\text{m}$, $0.64\mu\text{m}$ and $0.64\mu\text{m}$ respectively.

To investigate the influence of the length of spring-like leg, a dimensionless parameter, called leg-ratio, is used and defined as the ratio of spring-leg length to the total beam span. Figure 3(a) shows the simulated curves of displacement and flatness versus leg-ratio at 15 volts. The total beam span is $200\mu\text{m}$ long in simulation. Generally, larger leg-ratio shows larger displacement at fixed total beam span but limits the area of reflecting surface or the central beam portion. In addition, it is found the leg-ratio larger than 0.5 ensures that the central beam portion is almost un-deformed and remains flat beam profile during operation, as shown in figure 3(b). Therefore, the value of leg-ratio is chosen to be 0.6 in our designs that provides large optical reflecting surface and low actuation voltage to achieve the required displacement.

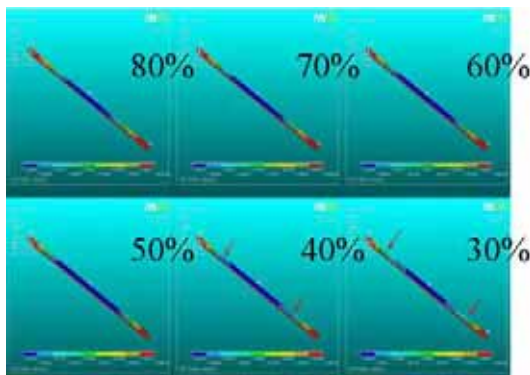
Figure 4 shows the simulated curves of displacement versus leg width for the case of $250\mu\text{m}$ long GLM2 at different values of air gaps between top and bottom electrodes. It is found the minimal displacements occur at leg width about $0.6\mu\text{m}$. Wider leg width has more affecting area of electrostatic force and stiffer leg structure. Therefore, for leg wider than $0.6\mu\text{m}$, electrostatic force increases more than that of leg stiffness and hence the displacement increases. However, wider leg width will cause the central beam portion deformed more at fixed leg-ratio. When the leg narrower than $0.6\mu\text{m}$, the stiffness of the leg decreases faster than the electrostatic force that increases displacement. In practical, the design rule restricts the minimum line width to $0.6\mu\text{m}$. Therefore, considering the displacement and flatness, leg widths in the range of $0.8\text{-}1.0\mu\text{m}$ are suitable for proposed GLMs with $3.0\mu\text{m}$ wide central beam portion.

Figure 5 shows the simulated deformed beam profiles of GLM1 and GLM2 at 162.5nm downward displacements ($1/4$ red light wavelength, λ_r) where the total beam span is $200\mu\text{m}$, leg-ratio is 0.6 and leg width is $1.0\mu\text{m}$. The radius of curvature of the conventional clamped-clamped beam (GLM1) is only $15.1\text{-}15.6\text{mm}$ that may cause large wavefront distortions. However, the proposed GLM2 has larger radius of $200\text{-}900\text{mm}$ that can provide flat reflective surfaces. The proposed GLM3 also shows flat beam profile as that of GLM2 but is not shown here.

The simulated static voltage-displacement curves of the $200\mu\text{m}$ long GLMs are shown in figure 6. The GLM2 requires 31.5V to exhibit 162.5nm displacements, which can be further, decreased by reducing the connected numbers of spring-like leg. The GLM3 with vertical comb electrodes shows lower actuation voltage of 16.2V to achieve 162.5nm displacements that is comparable to GLM1 at 13.7V . The gaps between comb fingers of the GLM3 are $0.65\mu\text{m}$ in simulation and fabrication.



(a)



(b)

Figure 3: (a) The effects of the ratio of spring-leg to total beam span. (Leg width = $1\mu\text{m}$, leg thickness = $0.925\mu\text{m}$) (b) The deformed shapes of the beams with various leg-ratios.

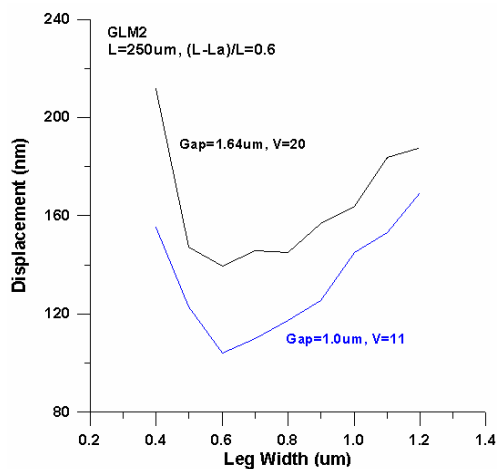


Figure 4: The effect of spring-like leg width on displacement. The width of central beam portion is $3\mu\text{m}$.

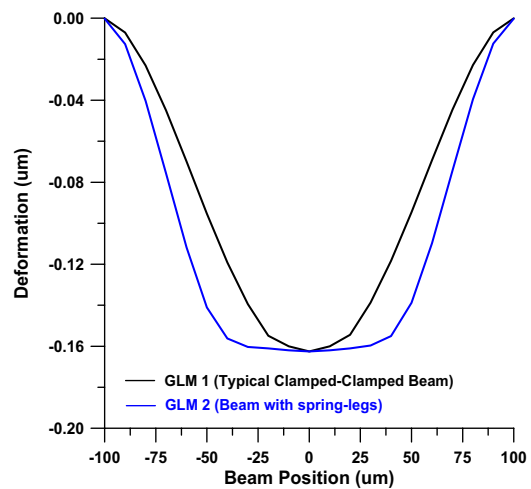


Figure 5: Beam deformation profiles of GLM1 and GLM2 (ratio of spring-leg length to the total beam span is 0.6). The GLM3 has similar profile as GLM2 and is not shown here.

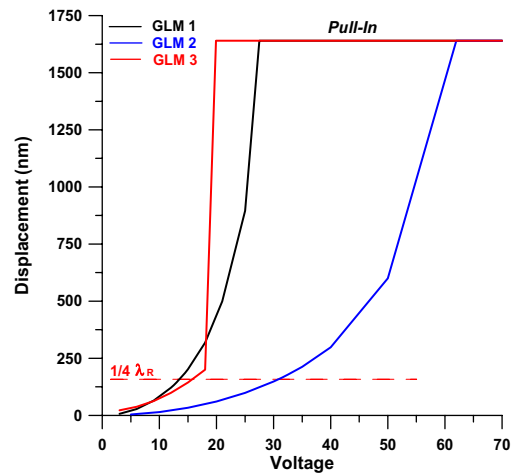


Figure 6: The voltage-displacement curves of GLM1, GLM2, and GLM3.

4 OPTICAL SIMULATIONS

The diffractive analyses of the grating light modulator are divided into the optical near field and the far-field propagation analyses. Owing to the CMOS fabrication process, the reflection effect of bottom electrode, called substrate reflectance, is considered in optical simulation with three different kinds of materials, aluminum, polysilicon and aluminum with tungsten dimples. The bottom aluminum electrode with tungsten dimples is developed here to reduce the stiction problem for the wet post CMOS process. Hence the possible effects of these dimples are also considered in optical simulation.

Figure 7(a) and 7(b) shows the simulated diffractive intensity contours of the grating light modulator before and after actuation with displacement of $1/4 \lambda_r$ at propagation

distance of $5000\mu\text{m}$. The gaps between ribbons, called inter-ribbon gap, are $0.6\mu\text{m}$ in simulation. In simulations, the existence of the inter-ribbon gap reduces 0^{th} mode diffractive efficiency from 100% (no gap) to 70% ($0.6\mu\text{m}$ gap). In addition, it is found that the three kinds of bottom electrodes show close diffractive intensity contours, as shown in figure 7(c). Therefore, the inclusion of simple structures does not affect the optical performance of the grating light modulators.

Due to substrate reflectance effect, the optimal value of inter-ribbon gap of $0.6\mu\text{m}$ is found to achieve maximum extinction ratio of the 1^{st} mode, as shown in figure 8. Figure 9 shows the optical intensity contours of the GLM1 and GLM2 actuated at $\lambda\pi/4$ displacements. The proposed GLM2 shows similar wavefront as the modulator with beams of zero curvature. Hence, the proposed designs GLM2 and GLM3 can improve the wavefront distortion significantly and has less energy residue at 0^{th} mode to only 1/3 of that caused by GLM1.

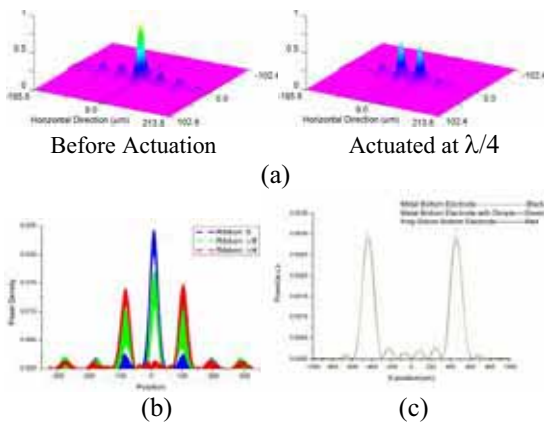


Figure 7: (a) Simulated diffractive intensity contours at propagation distance of $5000\mu\text{m}$. (b) Aluminum bottom electrode at 0 , $\lambda/8$ and $\lambda/4$ displacements; (c) comparisons of three kinds of bottom electrodes at $\lambda/4$ displacement.

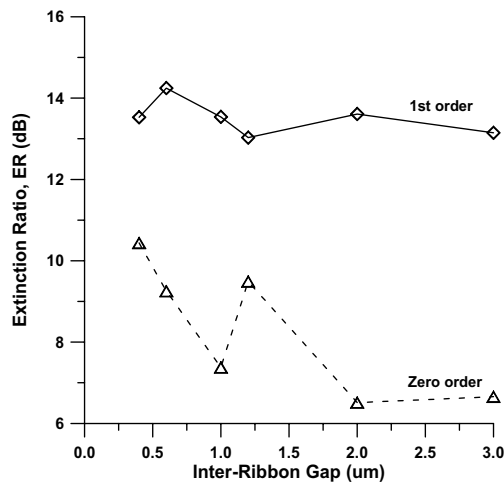


Figure 8: The extinction ratio v.s. inter-ribbon gap. (where beam width is $3.0\mu\text{m}$).

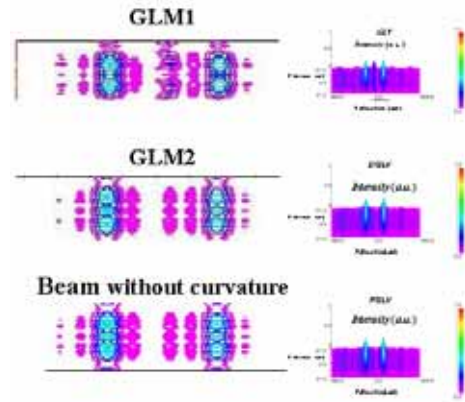


Figure 9: The GLM1 and GLM2 intensity distribution contours. The GLM2 improves wavefront similar to that of beams without curvature, hence shows less energy residue on 0^{th} mode.

5 CONCLUSIONS

Two new types of electrostatic grating light modulators (GLMs), one is actuated by parallel plate capacitor and the other is the vertical comb type, are proposed, designed, and analyzed to improve optical wavefront distortion. The gratings consist of parallel rows of rigid microbeam structures with proposed spring-like legs on beam-ends. The effect of length and width of the leg on the flatness and displacement of the proposed GLMs are discussed. Radius of curvature up to 200-900mm is achieved for $200\mu\text{m}$ long grating provides flat reflective surfaces. Optical simulations include the effect of bottom electrode reflection. Three kinds of bottom electrodes show close diffractive intensity contours. Simulated results indicate the proposed GLMs improve wavefront distortion significantly. The optimal gap-size between ribbons is found to be $0.6\mu\text{m}$.

REFERENCES

- [1] E. Tamaki, Y. Hashimoto and O. Leung, Proc. SPIE, v.6, 5348-8, 1-9, 2003.
- [2] J. I. Trisnadi, C. B. Carlisle and R. Monteverde, Photonics Wets 2004.
- [3] T. P. Kurzweg, J. A. Martinez and S. P. Levitan, Proc. SPIE, v.4985, 160-171, 2003.
- [4] E. P. Furlani, E. H. Lee and H. Luo, J. Appl. Phys. 83(2), 629-634, 1998.